The Kinematics of Containment for N-Dimensional Ellipsoids

Sipu Ruan
Department of Mechanical Engineering
The Johns Hopkins University,
Baltimore, MD 21218
Email: ruansp@jhu.edu

Jianzhong Ding
School of Mechanical Engineering and Automation
Beihang University, Beijing 100191, China
Email: jianzhongd@buaa.edu.cn

Qianli Ma
Aptiv Automotive, Pittsburgh, PA
Email: qianli.b.ma@aptiv.com

Gregory S. Chirikjian[*]
Department of Mechanical Engineering
National University of Singapore, Singapore 117575
Email: mpegre@nus.edu.sg
Department of Mechanical Engineering
The Johns Hopkins University, Baltimore, MD 21218
Email: gchirik1@jhu.edu

Knowing the set of allowable motions of a convex body moving inside a slightly larger one is useful in applications such as automated assembly mechanisms, robot motion planning, etc. The theory behind this is called the "Kinematics of Containment (KC)". In this article, we show that when the convex bodies are ellipsoids, lower bounds of the KC volume can be constructed using simple convex constraint equations. In particular, we study a subset of the allowable motions for an n-dimensional ellipsoid being fully contained in another. The problem is addressed in both algebraic and geometric ways, and two lower bounds of the allowable motions are proposed. Containment checking processes for a specific configuration of the moving ellipsoid and the calculations of the volume of the proposed lower bounds in configuration space (C-space) are introduced. Examples for the proposed lower bounds in 2D and 3D Euclidean space are implemented and the corresponding volumes in C-space are compared with different shapes of the ellipsoids. Practical applications using the proposed theories in motion planning problems and parts-handling mechanisms are then discussed.
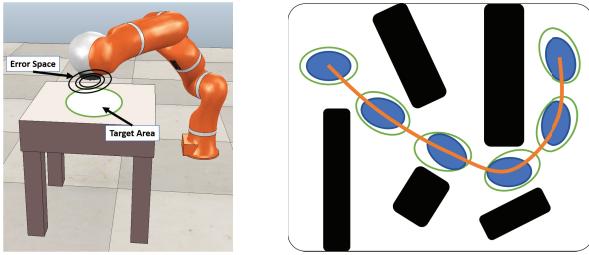
1 Introduction

Determining the allowable motions of an object in a structured environment is of interest in the field of robot motion planning [1], computer-aided design (CAD) [2], and automated assembly [3], etc. This problem can be interpreted as detecting whether an object in a specific pose (a position and orientation pair) is fully contained inside of a void, and computing how much volume such poses occupy in the whole configuration space (C-space).

1.1 Motivations

Concretely in an assembly task, for instance, a robot manipulator is picking an object and trying to assemble it into another part. Due to the errors propagated from each joint, even with a fixed input control signal, the pose of the end effector always has uncertainties. As a result, the union of the object at all possible ending poses formulates an *error*

(a) Parts-handling for a robot manipulator with errors on the end effector.

(b) Path planning for an elliptical mobile robot being enclosed by a larger elliptical void.

Fig. 1: Demonstration of the examples as motivations to the Kinematics of Containment theory.

space. The target area can be inscribed by ellipsoids, because of the simplicity of the shape that uses fewer parameters. Once the error space is fully contained inside the target area, the object can always be safely placed into the target. Further, the description of all the allowable motions in C-space of the object to be successfully placed into the target evaluates the robustness of the manipulator. Developing convenient methods for such problems would be helpful for the interval analysis of kinematic errors. And an important real-life application is the manipulators design for automated micro-assembly tasks, which requires precise robotic tools with guaranteed performance metric [4].

Furthermore, for a robot motion planning problem, as another example, sample-based planners such as PRM [5], RRT [6], RRT-Connect [7] have been well known for years and proved to be probabilistic complete and efficient in practice. However, large amounts of computations for collision detection between the robot and obstacles are required when dealing with narrow passage problems. Therefore, it is beneficial to develop efficient configuration construction and connection strategies in the C-space so that the traditional collision checking can be avoided. One of the solutions is to slightly enlarge the robot by a convex body so that it is able to move safely inside. Once a *convex* subspace of the space of all its allowable motions can be computed, any path inside that subspace is guaranteed to be collision-free. Then, connecting two safe configurations remains simply finding a path within the convex subspace.

Figure 1 demonstrates the assembly process and the motion planning problem described above, which motivates the work in this article.

1.2 The Goal of This Article

One way to query whether the moving ellipsoid at a specific configuration is in collision with the fixed one is to perform collision detection, where [8, 9] give fast ways to check collisions. Moreover, [10] computes the signed distance between two overlapping ellipsoids, which gives an algorithm to check whether one ellipsoid is contained in another. However, collision detection cannot fully describe the C-space of the allowable motions of the moving object, and this is where the concept of the Kinematics of Containment (KC) [11] fits

in.

The KC theory discusses how to identify and describe the allowable motions of a convex body being fully contained inside a slightly larger one, and provides an efficient way to compute the range of the restricted motions. The KC theory is further applied in [12], where a closed-form hyper-spherical representation as a lower bound for the allowable motions when the convex objects are ellipsoids was proposed. Based on those work, the contributions of this article are summarized as follows:

(1) Two lower bounds of the allowable motions based on the algebraic and geometric conditions of containment are developed respectively;

(2) Efficient containment checking process of a specific configuration for each lower bound is proposed;

(3) The computations of the occupied volumes for the two proposed lower bounds are performed and compared; and

(4) Applications in motion planning problems and parts-handling mechanisms are discussed.

The remainder of this article is organized as follows. In Section 2, we review the general concept of the Kinematics of Containment theory. Then in Section 3, we formulate the algebraic and geometric conditions for one *n*-dimensional ellipsoid being fully contained in another. Further in Section 4, we propose a convex lower bound for the allowable motions of the smaller ellipsoid based on the approximated algebraic condition of containment. In Section 5, we then propose a geometric lower bound based on the closed-form Minkowski difference between two ellipsoids. To make the lower bounds useful, in Section 6, we introduce the containment checking processes for the two lower bounds and the computations of the occupied volumes of allowable motions in C-space. In Sections 7 and 8, we perform numerical experiments in the 2D and 3D cases respectively, and compare the performance of the two proposed lower bounds. In Section 9, we discuss applications on a configuration connection strategy in a robot motion planning paradigm, and the error estimations and evaluations of a parts-handling task for a robot manipulator. We conclude in Section 10.

2 The Kinematics of Containment: A Review of the General Concepts

The Kinematics of Containment (KC) addresses the range of allowable motions for one convex body in $\mathbb{R}^n$ being completely inside of another, and provides a simple expression to compute the volume of such motions in the group of rigid-body motions, SE(n) [11]. The derivations are based on the Principal Kinematics Formula (PKF) [13, 14] from the field of integral geometry.

PKF studies the range of possible motions when two convex bodies, K_a and K_b in $\mathbb{R}^n$, intersect to each other. Such a range of motions can be characterized by the indicator function $\iota(\cdot)$, which is defined as 1 when the argument is nonempty and 0 otherwise. Therefore, when the two convex bodies intersect, i.e. $\iota(g \cdot K_a \cap K_b) = 1$ (assuming K_a is moving and K_b is fixed, $g \in$ SE(n) and $g \cdot K_a \doteq RK_a + \mathbf{t}$ defines the group action on the rigid body K_a, where $R \in$ SO(n) denotes

the orientation and $\mathbf{t} \in \mathbb{R}^n$ is the translation of the body), the volume of such motions can be computed as, when $n = 2$,

$$
\begin{aligned}
V_{PKF}^{\mathrm{SE}(2)} &= \int_{\mathrm{SE}(2)} \iota(g \cdot K_a \cap K_b) dg \\
&= 2\pi[\mathcal{A}(K_a) + \mathcal{A}(K_b)] + \mathcal{P}(\partial K_a) \cdot \mathcal{P}(\partial K_b),
\end{aligned}
\tag{1}
$$

where $\mathcal{A}$ and $\mathcal{P}$ are the area and perimeter of a planar object respectively, and dg is the bi-invariant integral measure for $\mathrm{SE}(n)$. When $n = 3$,

$$
\begin{aligned}
V_{PKF}^{\mathrm{SE}(3)} &= \int_{\mathrm{SE}(3)} \iota(g \cdot K_a \cap K_b) dg \\
&= 8\pi^2[\mathcal{V}(K_b) + \mathcal{V}(K_a)] + 2\pi\mathcal{F}(\partial K_b)\mathcal{M}(\partial K_a) \\
&\quad + 2\pi\mathcal{F}(\partial K_a)\mathcal{M}(\partial K_b),
\end{aligned}
\tag{2}
$$

where $\mathcal{V}$ is the volume of a spatial body, and $\mathcal{F}$ and $\mathcal{M}$ are the surface area and the integral of mean curvature of the bounding surface enclosing a spatial body respectively.

Different from PKF, the KC theory deals with the case when the moving K_a is completely contained inside K_b, i.e. $\iota(g \cdot K_a \subseteq K_b) = 1$. Then the volume of all possible motions of K_a can be expressed as, when $n = 2$,

$$
\begin{aligned}
V_{KC}^{\mathrm{SE}(2)} &= \int_{\mathrm{SE}(2)} \iota(g \cdot K_a \subseteq K_b) dg \\
&= 2\pi[\mathcal{A}(K_a) + \mathcal{A}(K_b)] - \mathcal{P}(\partial K_a) \cdot \mathcal{P}(\partial K_b),
\end{aligned}
\tag{3}
$$

and when $n = 3$,

$$
\begin{aligned}
V_{KC}^{\mathrm{SE}(3)} &= \int_{\mathrm{SE}(3)} \iota(g \cdot K_a \subseteq K_b) dg \\
&= 8\pi^2[\mathcal{V}(K_b) - \mathcal{V}(K_a)] - 2\pi\mathcal{F}(\partial K_b)\mathcal{M}(\partial K_a) \\
&\quad + 2\pi\mathcal{F}(\partial K_a)\mathcal{M}(\partial K_b).
\end{aligned}
\tag{4}
$$

The general KC theory provides the above clean and simple expressions for volume computations of the allowable motion space for arbitrary convex bodies.

Moreover, the volume expressions for the PKF and KC are also related to the Minkowski sum and difference between the two convex bodies with fixed orientations. Concretely and taking the volume of KC C-space as an example, the volume expression can be rewritten, for $\mathrm{SE}(n)$, as [11]

$$
\begin{aligned}
V_{KC}^{\mathrm{SE}(n)} &= \int_{\mathrm{SE}(n)} \iota(g \cdot K_a \subseteq K_b) dg \\
&= \int_{\mathrm{SO}(n)} \int_{\mathbb{R}^n} \iota(\mathbf{t} \cdot (R \cdot K_a) \subseteq K_b) d\mathbf{t} dR \\
&= \int_{\mathrm{SO}(n)} \mathcal{V}(K_b \ominus (R \cdot K_a)) dR,
\end{aligned}
\tag{5}
$$

where $\ominus$ denotes the Minkowski difference between two bodies.

The integrand is the volume of the Minkowski difference [15] between K_b and a rotated version of K_a, and the total volume of KC C-space can be computed by integrating over the rigid-body rotation group. Throughout this article, we specifically use Eq. (5) as a reference to evaluate the relative volumes of different lower bounds, denoted as the volume of the "actual" KC C-space. Note that Eq. (3)-(5) that extend from PKF to KC are heuristic with the following conditions being hold: the moving K_a is required to kiss the inner wall of K_b at one point while being fully contained at all orientations; in addition, the Minkowski difference between the two convex bodies is also required to exist at every orientation and be convex.

In the applications that motivate this work, not only the volume of motions is important, but getting a clear expression to describe that space plays another essential role. The latter problem can be addressed when the convex bodies are ellipsoids, where the actual motion space is lower bounded by the bounding volume. And the characterizations of such subspace are what this article mainly focuses on.

3 Mathematical Formulations: the Algebraic and Geometric Conditions of Containment

This section introduces the basic mathematical concepts that will be applied throughout the whole article, and provides both algebraic and geometric conditions for one n-dimensional ellipsoid being fully contained in another.

3.1 Configuration Space of an N-Dimensional Ellipsoid

An n-dimensional ellipsoid can be implicitly represented by $(\mathbf{x} - \mathbf{t})^\top A(\mathbf{x} - \mathbf{t}) = 1$, and the eigenvalue decomposition of $A = R\Lambda^{-2}(\mathbf{a})R^\top$ gives the semi-axis lengths and orientation of the ellipsoid, where $\Lambda(\cdot)$ denotes a diagonal matrix. This "inside-outside" equation can be applied to check whether a given point $\mathbf{x}_0$ is inside of the ellipsoid or not, i.e. the point is inside (in the interior or on the boundary of the ellipsoid) if $(\mathbf{x}_0 - \mathbf{t})^\top A(\mathbf{x}_0 - \mathbf{t}) \leq 1$. Further, the explicit expression can then be defined as $\mathbf{x} = R\Lambda(\mathbf{a})\mathbf{u} + \mathbf{t}$, which gives a quick way to sample a point on the boundary of the ellipsoid.

The allowable motions of the moving ellipsoid E_a can be described by the displacement of its center (as a translation $\mathbf{t} \in \mathbb{R}^n$) and the orientation (as a rotation $R \in \mathrm{SO}(n)$) with respect to the fixed ellipsoid E_b. Such a rotation and translation pair forms a Lie Group called "Pose Change Group" (PCG) as $(R, \mathbf{t}) \in \mathrm{PCG}(n) \doteq \mathrm{SO}(n) \times \mathbb{R}^n$ [16]. The corresponding Lie algebra can be obtained by logarithm map as $\xi = [\omega^\top, \mathbf{t}^\top]^\top \in \mathbb{R}^{n(n+1)/2}$. The Lie Algebra element can be transformed back to the Lie Group by exponential map, i.e. $(\exp(\widehat{\omega}), \mathbf{t}) \in \mathrm{PCG}(n)$ [1].

An element in $\mathrm{PCG}(n)$ specifies a configuration of the moving ellipsoid, and all of the configurations formulate the configuration space (C-space) [17]. The subset of the whole

---

[1] The mappings for the pose change group between the Lie Group and its Lie Algebra are different than the exponential and logarithm for $\mathrm{SE}(n)$.

C-space where the moving ellipsoid is fully contained in another fixed ellipsoid without any collision is denoted as the "Kinematics of Containment C-space (KC C-space)". The choice of PCG(n) provides a correct and natural way to represent a pose of the body and compute the change of poses as seen from the fixed world reference frame. In particular, the vector $\mathbf{t}$, which is the actual translation as seen in the world frame, remains the same when performing the exponential mappings between Lie group and Lie algebra. This is convenient from the computational aspect. On the other hand, for the conventional SE(n) representation, the translation part will change and have different meanings through the exponential maps.

Moreover, the volume computations of the KC C-space in PCG(n) follows the same fashion as in SE(n), where the rotation and translation parts can be split as

$$\int_{\text{PCG}(n)} f(R, \mathbf{t}) d\mathbf{t} dR = \int_{\text{SO}(n)} \int_{\mathbb{R}^n} f(R, \mathbf{t}) d\mathbf{t} dR, \qquad (6)$$

where $f(\cdot)$ denotes a general function.

3.2 The Algebraic Condition of Containment

The semi-axes of E_a and E_b are denoted as $\mathbf{a} = [a_1, a_2, ..., a_n]^\top, \mathbf{b} = [b_1, b_2, ..., b_n]^\top \in \mathbb{R}^n$ respectively. By substituting the explicit expression of the moving ellipsoid E_a into the implicit expression of the fixed ellipsoid E_b that is aligned with the world frame, the algebraic condition for E_a to move inside E_b without collision can be written as [12]

$$(R_a \Lambda(\mathbf{a})\mathbf{u} + \mathbf{t}_a)^\top \Lambda^{-2}(\mathbf{b})(R_a \Lambda(\mathbf{a})\mathbf{u} + \mathbf{t}_a) \leq 1, \qquad (7)$$

where $\mathbf{u}$ is the explicit expression of an n-dimensional sphere with $\|\mathbf{u}\| = 1$.

For this highly nonlinear expression, a small angle approximation can make it much simpler, where some better properties, such as convexity, can be proved. If the rotation of E_a is restricted, the rotation part calculated by exponential map can be approximated to the first order as

$$R_a = \exp(\widehat{\omega}_a) \approx \mathbb{I} + \widehat{\omega}_a, \qquad (8)$$

where $\mathbb{I} \in \mathbb{R}^{n \times n}$ denotes an identity matrix, $\omega \in \mathfrak{so}(n)$ is the Lie algebra of R, and $\hat{\cdot}$ denotes the "hat" operation that maps an n-dimensional vector into a skew-symmetric matrix.

Substituting Eq. (8) into Eq. (7) and grouping parameters ($\mathbf{u}$) and variables (ω and $\mathbf{t}$) gives the approximation of the left-hand side of the algebraic condition of containment as

$$C_\mathbf{u}(\xi) \doteq \xi^\top H(\mathbf{u})\xi + \mathbf{h}^\top(\mathbf{u})\xi + c(\mathbf{u}), \qquad (9)$$

where $H(\mathbf{u}) \in \mathbb{R}^{n(n+1)/2 \times n(n+1)/2}$, $\mathbf{h}(\mathbf{u}) \in \mathbb{R}^{n(n+1)/2}$ and $c(\mathbf{u}) \in \mathbb{R}$. The first order algebraic condition of containment

Table 1: Confusion matrix for the actual algebraic condition in Eq. (7) of containment and its approximation in Eq. (10).

Actual	Approx. (2D)		Actual	Approx. (3D)	
(2D)	True	False	(3D)	True	False
True	1858	1771	True	2404	951
False	0	6371	False	0	6645

is then defined as

$$C_\mathbf{u}(\xi) \leq 1. \qquad (10)$$

The approximation is a subset (or a lower bound) of the actual algebraic condition of containment in the sense that Eq. (10) implies Eq. (7) and the reverse is not true. This statement is verified by numerically sampling 10000 random configurations and testing the status of Eq. (7) and Eq. (10) respectively. The result is shown as a confusion matrix in Tab. 1 for both the 2D and 3D cases. From the experiment, when the approximation returns "True" (E_a is fully contained in E_b), the actual containment condition is always "True", which implies that all the configurations that satisfy the approximation also satisfy the actual algebraic condition of containment.

3.3 The Geometric Condition of Containment

The KC C-space boundary can also be determined in a geometric way: For each fixed orientation of E_a, the trajectory of its center when just touching E_b is generated by the Minkowski difference between the two ellipsoids. And the whole actual KC C-space boundary can be constructed as a union of those Minkowski differences at all possible orientations.

For two *n*-dimensional ellipsoids, the Minkowski difference can be calculated in explicit closed-form efficiently [18], by first shrinking E_a into a sphere (E_a') and computing an offset curve. The constraint for such derivation requires the curvature of the ellipsoid at every point after shrinking must be smaller than the curvature of the sphere. Another implementation for Minkowski difference between two ellipsoids is introduced in Ellipsoidal Toolbox [19], which is used throughout this paper to generate the exact KC C-space as a reference for comparison.

The explicit boundary of the Minkowski difference cannot be applied directly in the KC theory, because it is nontrivial to determine whether a point is inside only from the knowledge of the parametric boundary expression. As a result, it is important to find a lower bound for the KC C-space that has a simple expression, making such a querying process easy and fast. Inspired by the shrinking process in the closed-form solutions, a geometric lower bound can be obtained from computing the extreme distance for the sphere to move along each semi-axis of the ellipsoid in the shrunk space.

4 A Convex Lower Bound Based on the Approximated Algebraic Condition of Containment

This section starts from showing that the approximation of the algebraic condition is convex, so that given some configurations, the interior of their convex hull is a safe subset and can be treated as a lower bound of the KC C-space. Then this convex lower bound can be constructed as a convex polyhedron using several extreme vertices.

4.1 Convexity of the Approximated Algebraic Condition of Containment

The approximated algebraic condition must be satisfied over all $\mathbf{u}_i$ in the unit sphere, which is equivalent to

$$\max_{\forall \mathbf{u}_i} C_i(\xi) = \max_{\forall \mathbf{u}_i}[\xi^\top H(\mathbf{u}_i)\xi + \mathbf{h}(\mathbf{u}_i)^\top \xi + c(\mathbf{u}_i)] \leq 1 \quad (11)$$

We first show that the left-hand side of (11) is convex as follows.

Proof. For any fixed $\mathbf{u}_i$ ($i = 1, ..., m$), given $\xi_1, \xi_2 \in \mathbb{R}^{n(n+1)/2}$,

$$
\begin{aligned}
&C_i(\alpha\xi_1 + (1-\alpha)\xi_2) - [\alpha C_i(\xi_1) + (1-\alpha)C_i(\xi_2)] \\
=&[(\alpha\xi_1 + (1-\alpha)\xi_2)^\top H(\mathbf{u}_i)(\alpha\xi_1 + (1-\alpha)\xi_2) \\
&+ \mathbf{h}(\mathbf{u}_i)^\top(\alpha\xi_1 + (1-\alpha)\xi_2) + c(\mathbf{u}_i)] \\
&-[\alpha(\xi_1^\top H(\mathbf{u}_i)\xi_1 + \mathbf{h}(\mathbf{u}_i)^\top\xi_1 + c(\mathbf{u}_i)) \\
&+ (1-\alpha)(\xi_2^\top H(\mathbf{u}_i)\xi_2 + \mathbf{h}(\mathbf{u}_i)^\top\xi_2 + c(\mathbf{u}_i))] \\
=&-\alpha(1-\alpha)[(\xi_1 - \xi_2)^\top H(\mathbf{u}_i)(\xi_1 - \xi_2)], \forall\alpha \in [0,1].
\end{aligned}
\quad (12)
$$

The above expression is non-positive if and only if $(\xi_1 - \xi_2)^\top H(\mathbf{u}_i)(\xi_1 - \xi_2) \geq 0$, or equivalently, $H(\mathbf{u}_i)$ is symmetric positive semi-definite. By direct calculations for the quadratic part, we have, $\forall\xi \in \mathbb{R}^{n(n+1)/2}$,

$$\xi^\top H(\mathbf{u}_i)\xi = (\widehat{\omega}_a\Lambda(\mathbf{a})\mathbf{u}_i + \mathbf{t}_a)^\top \Lambda^{-2}(\mathbf{b})(\widehat{\omega}_a\Lambda(\mathbf{a})\mathbf{u}_i + \mathbf{t}_a). \quad (13)$$

Since $\Lambda^{-2}(\mathbf{b})$ is diagonal with non-negative entries on diagonal, Eq. (13) ≥ 0, which means that $H(\mathbf{u}_i)$ is symmetric and positive semi-definite. Hence, each condition function $C_i(\xi)$ is convex. And since maximization preserves convexity [20], $\max C_i(\xi)$ is convex, which concludes the proof.

From the convexity of $\max C_i(\xi_j)$, if for two extreme points ξ_1, ξ_2, $\max C_i(\xi_j) \leq 1, j = 1, 2$ hold, then for points on the line segment between them, $\alpha\xi_1 + (1-\alpha)\xi_2, \forall\alpha \in [0,1]$, $\max C_i(\alpha\xi_1 + (1-\alpha)\xi_2) \leq \alpha\max C_i(\xi_1) + (1-\alpha)\max C_i(\xi_2) \leq 1$ is also satisfied. Hence points inside the convex hull of the extreme points also satisfy the approximated algebraic condition of containment.

4.2 Finding extreme vertices that represent the polyhedron

Now we search for the extreme points of the polyhedron by the following 2 cases: (1) extreme points that lie on each

axis of the C-space; (2) points that have the largest magnitude.

Extreme points in each axis can be simply found by fixing the other axis lengths to zero. Since in each axis, there are 2 extreme points (positive and negative), we get $2n$ points for the first case, where n is the dimension of the configuration space.

For the vertices that have largest magnitude, we seek to maximize the squared norm of ξ, with the constraint being the algebraic condition as

$$\xi^* = \arg\max \xi^\top\xi \quad \text{s.t. } C_i(\xi) \leq 1 \quad (i = 1, ..., m). \quad (14)$$

Since the objective function is quadratic, the solutions for each variable have 2 possibilities, so the total number of solutions can be up to 2^n. However, not all of those possibilities are feasible solutions, meaning that we have to validate them by substituting back to the constraint inequalities.

5 A Geometric Lower Bound Based on the Minkowski Difference between Two Ellipsoids

In this section, we first review and derive a more explicit expression for the closed-form Minkowski difference between two ellipsoids. Further, a convex polyhedron as a lower bound for the Minkowski difference boundary is developed by computing the extreme points at each semi-axis of the ellipsoid in the shrunk space.

5.1 Review of the Closed-Form Minkowski Difference between Two N-Dimensional Ellipsoids

The closed-form Minkowski difference between two ellipsoid first applies an affine transformation to shrink the smaller ellipsoid E_a into a sphere E_a' with radius $r \doteq \min(a_1, a_2, ..., a_n)$ [18]. The resulting space is denoted as a "shrunk space", and the original E_b is transformed into E_b' as

$$\mathbf{x}' = R_a\Lambda^{-1}(\mathbf{a}/r)R_a^\top\mathbf{x} \doteq T^{-1}\mathbf{x}, \quad (15)$$

where $T = R_a\Lambda(\mathbf{a}/r)R_a^\top$.

The implicit expression for the boundary of E_b' is $\Phi(\mathbf{x}') = \mathbf{x}'^\top B'^{-2}\mathbf{x}' = 1$, where $B'^{-2} = TB^{-2}T$. The Minkowski difference between E_b' and E_a' can be obtained by computing the offset surface with offset radius r as

$$\mathbf{x}_{ofs} = \mathbf{x}' - r\mathbf{n}', \quad (16)$$

where $\mathbf{n}' = \frac{\nabla\Phi(\mathbf{x}')}{\|\nabla\Phi(\mathbf{x}')\|}$ is the outward normal of the surface and $\nabla\Phi(\mathbf{x}') = 2B'^{-2}\mathbf{x}'$. Then the Minkowski difference between the two ellipsoids E_a and E_b can be given by "stretching" (inverse of the previous affine transformation) the shrunk space
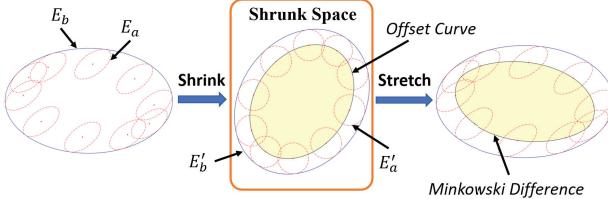
Fig. 2: Demonstration of the computational procedure of the closed-form Minkowski difference between two ellipsoids.

back as

$$
\begin{aligned}
\mathbf{x}_{eb} = T\mathbf{x}_{ofs} = T(\mathbf{x}' - r\mathbf{n}') &= T(T^{-1}\mathbf{x} - r\frac{TB^{-2}TT^{-1}\mathbf{x}}{\|TB^{-2}TT^{-1}\mathbf{x}\|}) \\
&= \mathbf{x} - r\frac{T^2B^{-2}\mathbf{x}}{\|TB^{-2}\mathbf{x}\|} = B\mathbf{u}(\phi) - r\frac{T^2B^{-1}\mathbf{u}(\phi)}{\|TB^{-1}\mathbf{u}(\phi)\|}.
\end{aligned}
$$
(17)

The computational procedure is demonstrated in Fig. 2.

5.2 Extreme Distance that a Sphere Can Move Along Each Semi-Axis of an Ellipsoid in $\mathbb{R}^n$

Inspired by the derivations above, the geometric lower bound can be obtained from the extreme distance that E'_a can move along each semi-axis of E'_b in the shrunk space. It can be further observed E'_b is still an ellipsoid, whose semi-axis length and orientation can be computed by eigenvalue decomposition of the transformed shape matrix $T\Lambda^{-2}(\mathbf{b})T = R'\Lambda^{-2}(\mathbf{b}')R'^\top$. For simplicity, E'_b is further rotated by $R'^\top$ to align with the world frame. The extreme distance at each semi-axis happens when E'_a just touches E'_b, the condition of which is stated as follows.

Suppose $\mathbf{x}_0 = [x_1, x_2, ..., x_n]^\top \in \partial E_{b'}$ is a point on the ellipsoid surface, it should also be on the surface of the sphere, and the outward normals of both surfaces at $\mathbf{x}_0$ should lie on the same line. Then, the problem becomes simultaneously solving

$$
\mathbf{x}_0^\top \Lambda^{-2}(\mathbf{b}')\mathbf{x}_0 = 1, \tag{18a}
$$

$$
(\mathbf{x}_0 - d\mathbf{e}_i)^\top(\mathbf{x}_0 - d\mathbf{e}_i) = r^2, \tag{18b}
$$

$$
2\Lambda^{-2}(\mathbf{b}')\mathbf{x}_0 = 2k(\mathbf{x}_0 - d\mathbf{e}_i), \tag{18c}
$$

where d is the extreme distance at the ith semi-axis, and k is a scalar indicating the outward normal of both surfaces lies on the same line. The solution can be obtained as

$$
d_i^* = \begin{cases} \dfrac{1}{b'_{j*}}\sqrt{\left(b_{j*}'^2 - b_i'^2\right)\left(r^2 - b_{j*}'^2\right)}, & r \geq b_{j*}'^2/b_i' \\ b_i' - r, & r < b_{j*}'^2/b_i', \end{cases} \tag{19}
$$

where $j^* = \arg\max_{j\neq i}(b'_j)$.

Proof. Without loss of generality, we limit the range of the extreme distance to be $d_i^* \in [0, b_i' - r]$. The upper bound, which is the largest distance that E'_a can move along each semi-axis. Expanding Eq. (18c) and defining $B' \doteq \Lambda^{-2}(\mathbf{b}')$ gives

$$
(B - k\mathbb{I})\mathbf{x}_0 = -kd\mathbf{e}_i. \tag{20}
$$

Since $B - k\mathbb{I}$ is diagonal, Eq. (20) holds in just two cases:
(I) $\mathbf{x}_0 = x_i\mathbf{e}_i$ ($x_i \neq 0$); or
(II) $\mathbf{x}_0 = x_i\mathbf{e}_i + \sum_j x_j\mathbf{e}_j$, where $\forall j, k = b_j'^{-2}$ ($i \neq j$, $x_i, x_j \neq 0$). Geometrically, case (I) or (II) happens when the vector from origin to the touching point is or is not parallel to the ith semi-axis respectively. As a result, those two cases cover all possible situations of the solution.

Case (I): when $\mathbf{x}_0 = x_i\mathbf{e}_i$ ($x_i \neq 0$), Eq. (18a) and (18b) become $x_i^2 b_i'^{-2} = 1$ and $d^2 - 2x_i d + x_i^2 - r^2 = 0$ respectively. Solving for d gives $d = x_i \pm r = \pm b_i' \pm r$. Combining with the range of the extreme distance, we have

$$
d_i^* = b_i' - r. \tag{21}
$$

Case (II): Substituting $\mathbf{x}_0$ into Eq. (18a) and (18b) gives

$$
\sum_j (x_j^2 b_j'^{-2}) + x_i^2 b_i'^{-2} = 1, \tag{22a}
$$

$$
\sum_j (x_j^2) + (x_i - d)^2 = r^2. \tag{22b}
$$

Since $\forall j, b_j'^{-2} = k$ are the same, it can be grouped out from the summation in Eq. (18a) as

$$
b_j'^{-2}\sum_j (x_j^2) + x_i^2 b_i'^{-2} = 1. \tag{23}
$$

Further, by substituting the equation for the sphere into the equation for the ellipsoid, we obtain
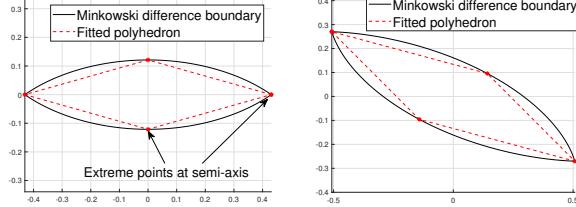
$$
b_j'^{-2}[r^2 - (x_i - d)^2] + x_i^2 b_i'^{-2} = 1. \tag{24}
$$

Using the condition $k = b_j'^{-2}$, Eq. (20) becomes

$$
(b_i'^{-2} - b_j'^{-2})x_i = -b_j'^{-2}d, \tag{25}
$$

where x_i and b_i' are fixed since the touching points are fixed once the shapes of the ellipsoid and sphere are given. The index j can be searched when b'_{j*} is the maximum of all the semi-axes other than b_i', because the extreme distance should be the minimum among all possible values. Therefore we have

$$
j^* = \arg\max_{j\neq i}(b'_j). \tag{26}
$$

(a) Extreme points in the shrunk space.

(b) Transformed extreme points in the actual C-space.

Fig. 3: Demonstration of polyhedron lower bound for Minkowski difference boundary in the shrunk space and actual C-space.

Combining Eq. (24), (25) and (26) and solving for d gives

$$d_i^* = \frac{1}{b'_{j*}} \sqrt{\left(b'^2_{j*} - b'^2_i\right)\left(r^2 - b'^2_{j*}\right)}. \tag{27}$$

The critical value of the radius r between the two cases can be calculated by equating (21) and (27) as

$$r = b'^2_{j*}/b'_i. \tag{28}$$

And from the geometric point of view, when r is less than this critical value, the sphere should touch the end point of the ellipsoid at the ith semi-axis, which is in case (I); otherwise, we should compute the extreme distance according to case (II).

5.3 Polyhedron as a Lower Bound for the Minkowski Difference Boundary at Each Orientation of the Moving Ellipsoid

From the result (19), a convex polyhedron in the shrunk space can be constructed by the extreme points at each semi-axis of the ellipsoid. The polyhedron is guaranteed to be in the interior of the true Minkowski difference boundary since Minkowski difference between two convex sets are convex. Also, since affine transformation preserves the convexity [20], transforming back from the shrunk space still gives a convex polyhedron which is a lower bound for the Minkowski difference between the two original ellipsoids. Figure 3 shows the idea of polyhedron lower bound for the Minkowski difference in the shrunk space and the actual C-space.

The polyhedron introduced above is defined at one specific orientation of the moving ellipsoid, and the union of the polyhedron subset at all orientations of E_a formulates the geometric lower bound of the KC C-space. Note that, this lower bound is no longer a convex polyhedron any more, but it is relatively simple in terms of querying an interior point and computing the volume.

6 Containment Checking and Volume Computations for the Lower Bounds of KC C-space

This section gives a review of how to query a point $P_{test} \in \mathbb{R}^n$ inside a polyhedron and compute the volume of such an n-dimensional polyhedron. The processes can be directly applied for the *Convex Lower Bound*, and extended for the *Geometric Lower Bound*.

Suppose the convex polyhedron is constructed by m vertices $\{P_i\} \in \mathbb{R}^n, i = 1,...,m$. It can be decomposed into a union of disjoint simplexes in $\mathbb{R}^n$ by Delaunay triangulation [21]. For each simplex with $n+1$ vertices, i.e. $P_i^s (i = 0,...,n)$, the point inside should satisfy

$$P_{test} = \sum_{i=0}^{n} \lambda_i P_i^s, \text{ where } \lambda_i \in [0,1] \text{ and } \sum_{i=0}^{n} \lambda_i = 1. \tag{29}$$

This condition can be formed in matrix form as

$$\begin{bmatrix} P_{test} \\ 1 \end{bmatrix} = \begin{bmatrix} P_0^s & P_1^s & \cdots & P_n^s \\ 1 & 1 & \cdots & 1 \end{bmatrix} \begin{bmatrix} \lambda_0 & \lambda_1 & \cdots & \lambda_n \end{bmatrix}^\top, \ \lambda_i \in [0,1](\forall i) \tag{30}$$

The point P_{test} is inside the simplex if the solution of the matrix equation Eq. (30), $[\lambda_0,...,\lambda_n]^\top$, satisfies $\lambda_i \in [0,1](\forall i)$. Further, this point is inside the polyhedron if it is inside any decomposed simplex.

Given the vertices of a convex polyhedron, the volume can be computed as a sum of all the volumes of the decomposed simplexes as

$$\mathcal{V}_{poly} = \sum_{i=1}^{m} \mathcal{V}_{simplex}^{(i)}(P_0^s, P_1^s, ..., P_n^s), \tag{31}$$

where $\mathcal{V}_{simplex}^{(i)}(P_0^s, P_1^s, ..., P_n^s)$ denotes the volume of the i-th simplex with $n+1$ vertices $P_0^s, P_1^s, ..., P_n^s$. The volume of a simplex in $\mathbb{R}^n$ defined by the $n+1$ vertices can be calculated as [22]

$$\mathcal{V}_{simplex} = \left\| \frac{1}{n!} \det(P_1^s - P_0^s, P_2^s - P_0^s, ..., P_n^s - P_0^s) \right\| \tag{32}$$

For the Convex Lower Bound, the above computations can be applied directly; and further for the Geometric Lower Bound, since at each fixed orientation, the KC C-space is a convex polyhedron, the same process can be used.

The containment checking for the Geometric Lower Bound is given as follows: once a configuration $\xi_{test} = [\omega_{test}^\top, \mathbf{t}_{test}^\top]^\top$ is given, we first transform the whole space via the knowledge of ω_{test}, and query the translation part $\mathbf{t}_{test}$ configuration in the shrunk space. For the volume, since the polyhedron vertices are aligned with the semi-axes of the ellipsoid, and the two vertices on one semi-axis are symmetry about the origin, the volume of the polyhedron becomes

$$\mathcal{V}'_{geo}(R_a) = \frac{2^n}{n!} \prod_{i=1}^{n} d_i^*. \tag{33}$$

The actual volume after the inverse affine transformation can be computed as

$$\mathcal{V}_{geo}(R_a) = \det(TR_a')\,\mathcal{V}'_{geo}(R_a) = \frac{2^n}{n!}\,|\Lambda(\mathbf{a}/r)|\prod_{i=1}^{n}d_i^*. \quad (34)$$

The volume computed at each orientation of E_a is a function of the rotation group, so the total volume can be calculated by integration over all rotations as

$$V_{total} = \int_R \mathcal{V}_{geo}(R)dR. \quad (35)$$

Explicitly for the case $SO(2)$,

$$V_{total}^{SO(2)} = \int_{-\pi}^{\pi}\mathcal{V}_{geo}(\theta)d\theta; \quad (36)$$

and for the case $SO(3)$,

$$V_{total}^{SO(3)} = \int_{\|\omega\|<\pi}\mathcal{V}_{geo}(R(\omega))|\det(J(\omega))|d\omega, \quad (37)$$

where analytically $|\det(J(\omega))| = \frac{2(1-\cos\|\omega\|)}{\|\omega\|^2}$ [23].

7 Numerical Experiments in 2D

This section simulates the proposed convex and geometric lower bounds for the KC C-space in one rigid body 2D ellipse case. We define $\mathbf{a} = [a_1, a_2]^\top$ and $\mathbf{b} = [b_1, b_2]^\top = (1+\varepsilon)\mathbf{a}$ as the semi-axis lengths of the moving and fixed ellipses E_a and E_b. The constrained motion of E_a within E_b is described as a rotation and translation pair $(R, \mathbf{t}) \in PCG(2)$. For the convex lower bound which applies the algebraic conditions, the expressions of matrix H, vector $\mathbf{h}$ and scalar c have been calculated explicitly in [12]. And for visualization and comparison purposes, we construct the shape of the true Minkowski difference boundary to illustrate the relationships between the actual KC C-space and the two proposed lower bounds. All the experiments are implemented in Matlab 2017a and run in an Intel Core i7-4790 CPU @ 3.60GHz.

7.1 Visualizations and Containment Checking Validations of the Two Lower Bounds

The Convex Lower Bound is construct by first finding extreme points at each C-space axis as follows. For the two translational axis (x and y), the extreme points are located at $x_{ex} = \pm\varepsilon a_1$ and $y_{ex} = \pm\varepsilon a_2$ respectively. For the rotational axis (θ), the extreme points can be found, in closed-form, as $\theta_{ex} = \arctan(\theta_y/\theta_x)$, where

$$\theta_x = \sqrt{(1+\varepsilon+\alpha)(1+\varepsilon-\alpha)(1+\alpha(1+\varepsilon))(1-\alpha(1+\varepsilon))} \quad (38a)$$

$$\theta_y = \alpha\varepsilon(2+\varepsilon) \quad (38b)$$

(a) Convex lower bound by 10 extreme vertices. Blue dots: the extreme configurations; Shaded area: the convex polyhedral lower bound.

(b) Ellipses at the 10 extreme configurations. Blue ellipses: ellipses with the extreme configurations; Red asterisks: centers of the blue ellipses.
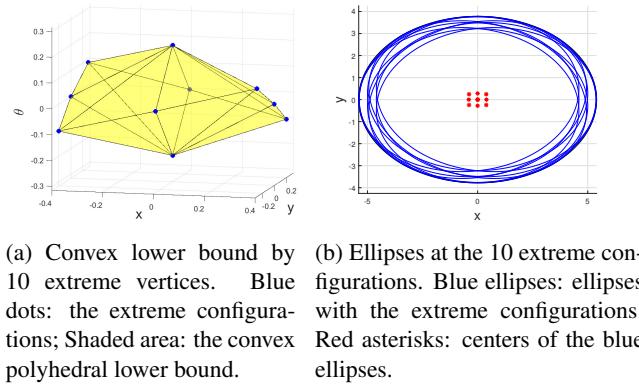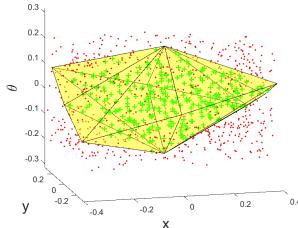
Fig. 4: Visualizations for the Convex Lower Bound.
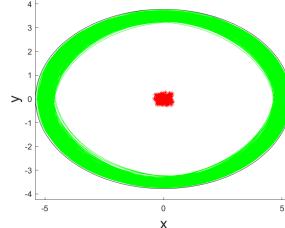
Note that this solution can be found by equating the implicit expressions of the two ellipsoids. Then, for the points with largest magnitude, we apply the convex constraint optimization with $\xi = [\theta, x, y]^\top$. Note that we might get 8 results since the cost function is quadratic, only 4 of them are valid by plugging back into the constraint functions. Thus, in total, we now get 10 extreme points to construct the polyhedron subspace from the configuration space.

Figure 4a demonstrates the proposed convex lower bound in C-space as a polyhedron made by 10 extreme vertices, which are plotted as big dots, and Fig. 4b plots the small ellipses in Euclidean space which are at the extreme configurations. To check the validity of the convex lower bounds, Fig. 5 shows the numerical results of the "point-in-polyhedron" test for 1000 randomly sampled configurations for E_a. Further, the ellipses whose configurations are inside the polyhedron are checked for collision with the larger ellipse using Eq. (7) numerically. The configuration points inside are indicated as plus signs while those in collision are marked as dots. The corresponding ellipses with those safe configurations are drawn in green whose center are marked as red asterisks. This visualization, along with the collision checking criteria, numerically verifies that the proposed convex lower bound gives the collision-free space and the querying procedure is numerically correct.

The same sampling and containment checking procedure are performed for the geometric lower bound. Figure 6a demonstrates the containment checking process with 1000 sampled configurations, and the numerical collision checking are performed for each safe configuration for a double confirmation. The blue dashed surface visualizes the shape of the geometric lower bound, where we uniformly sample the rotational angles between the maximum and minimum allowable angles. The number of the angles does not play an important role, since it does not affect the containment checking process. Plus signs and dots indicates the collision-free and in-collision configurations, respectively. Figure 6b shows the safe poses of the smaller ellipsoid in Euclidean space.
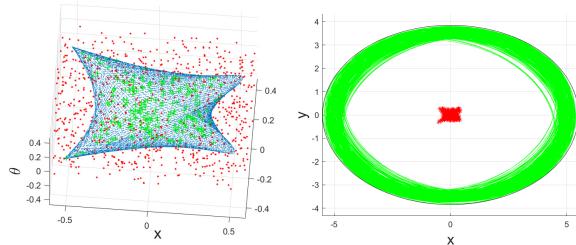
(a) Convex lower bound with sampled configurations. Dots: outside the polyhedron; plus signs: safe configurations inside the polyhedron.
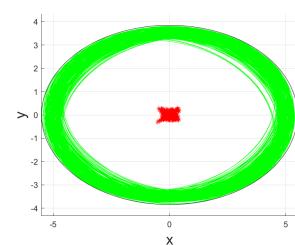
(b) Ellipses with the safe configurations. Green ellipses: ellipses with safe configurations; Red asterisks: centers of the green ellipses.

Fig. 5: Validation of the containment checking procedure for Convex Lower Bound.

(a) Geometric lower bound with sampled configurations. Dots: outside the lower bound; plus signs: safe configurations inside the lower bound.

(b) Ellipses with the safe configurations inside the geometric lower bound. Green ellipses: ellipses with safe configurations; Red asterisks: centers of the green ellipses.
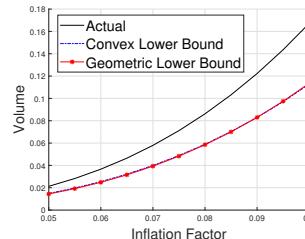
Fig. 6: Validation of the containment checking procedure for Geometric Lower Bound.

7.2 Volume Comparisons of Different Lower Bounds
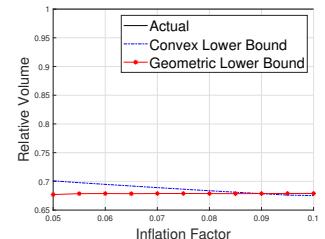
Numerical computations of the volume for each method are compared. And both the absolute and relative volumes with respect to the actual KC C-space are calculated. For the actual KC C-space, the volume is computed by integrating the volume of the actual Minkowski difference between the two ellipses over $SO(2)$ using Eq. (5).

The experiments are performed by: (1) varying the inflation factor ε between E_a and E_b with the semi-axis lengths fixed as $\mathbf{a} = [5, 3.5]^\top$ and $\mathbf{b} = (1+\varepsilon)\mathbf{a}$; and (2) varying the aspect ratio $\alpha = a_1/a_2$ for E_a with fixed longer semi-axis length at $a_1 = 5$ and inflation factor at $\varepsilon = 0.08$.

Figure 7 shows the volume comparisons of the KC C-space for different methods, where Fig. 7a shows the absolute volume and Fig. 7b shows the relative volumes compared to the one generated by the Minkowski difference. The convex lower bound occupies a slightly larger space when the inflation factor is small, but becomes smaller as the inflation factor increases. This indicates that the small angle assumption and the first-order approximation works well when the rotation is restricted, but drops accuracy when there is
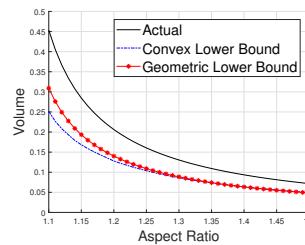
(a) Absolute volume.
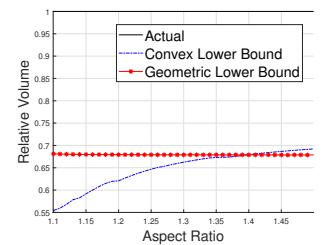
(b) Relative volume.

Fig. 7: Comparisons in 2D for the volumes of different lower bounds of the KC C-space with different inflation factors.

(a) Absolute volume.
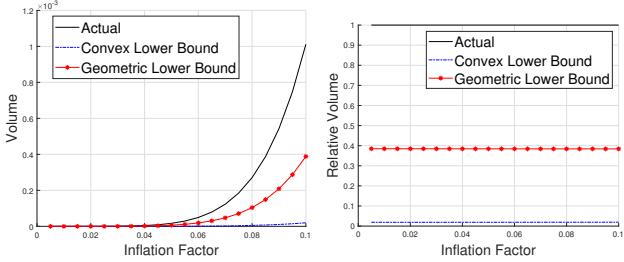
(b) Relative volume.

Fig. 8: Comparisons in 2D for the volumes of different lower bounds of the KC C-space with different aspect ratios.

more freedom for E_a to rotate. The geometric lower bound, on the other hand, performs more stable in terms of the relative volume. This shows that the polygon generated by extreme points at each semi-axis is a good choice to approximate the Minkowski difference boundary in the shrunk space.

Figure 8a compares the volume for different methods with the aspect ratio of the ellipse varying at the range $\alpha \in [1.1, 1.5]$, and Fig. 8b shows the relative volumes with the one generated by Minkowski difference. As the aspect ratio increases, the volume of allowable motion decreases, but the relative volume for the convex lower bound increases. When the aspect ratio is close to 1, the ellipses are close to circles, and so E_a has more free space to rotate, which makes the first-order approximation less accurate, and the convex lower bound performs worse. But the geometric lower bound still works much more stable with the changes of the aspect ratio.

8 Numerical Experiments in 3D

We further perform experiments for 3D ellipsoid case, whose configuration space is now 6 dimensional, i.e $\xi = [\omega_1, \omega_2, \omega_3, x, y, z]^\top \in \mathbb{R}^6$. Since it is not possible to visualize a 6D space, we only perform the query process for sampled configurations and do the collision checking as a double confirmation for each method; and compute the volume of each lower bound of KC C-space for comparisons.

(a) Absolute volume.   (b) Relative volume.

Fig. 9: Comparisons in 3D for the volumes of different lower bounds of the KC C-space with different inflation factors.

(a) Absolute volume.   (b) Relative volume.

Fig. 10: Comparisons in 3D for the volumes of different lower bounds of the KC C-space with different aspect ratios.

8.1 Containment Checking Validations of the Two Lower Bounds
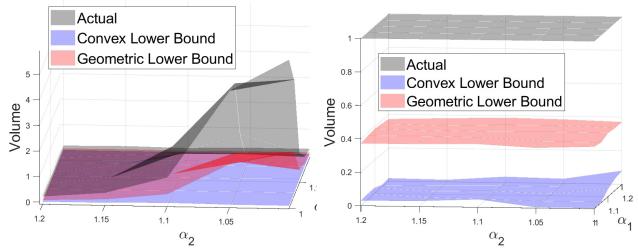
The extreme points in translation axes are, similar to 2D, $x_{extreme} = \pm\varepsilon a_1$, $y_{extreme} = \pm\varepsilon a_2$ and $z_{extreme} = \pm\varepsilon a_3$ respectively. To find the extreme points in rotational axes, we project the 3D space onto the x,y-, x,z-, y,z- plane. So the problem shrinks to the 2D case of finding the extreme rotational points at each plane, then the number of extreme points is 12. The extreme points with largest magnitude can be obtained by the constraint convex optimization from Eq. (14), which gives 64 possible solutions and only 32 are valid. Combined with the extreme points at each axis, in total, we get 44 extreme points to create the 6D polyhedron. For numerical validations, we also randomly sample 1000 configurations, and query those points in the 6D polyhedron. The results are compared with the collision detection based on the exact algebraic condition of containment to verify our theory.

For the geometric lower bound, we first compute the orientation of each of the 1000 sampled configurations, and check whether the translation part is inside the polyhedron lower bound for the Minkowski difference boundary. Further validations of the exact algebraic condition of containment are performed for double confirmation.

8.2 Volume Comparisons of the Two Lower Bounds

The volumes of the lower bounds with respect to inflation factors and aspect ratios are compared. For the inflation factors, the semi-axis lengths of E_a are set to be $\mathbf{a} = [4, 2.5, 2]^\top$, and the inflation factors vary within the range of $\varepsilon \in [0.01, 0.2]$. Figure 9 shows the volume comparisons between different lower bounds with respect to the inflation factor. The geometric lower bound occupies a much larger volume of the KC C-space than the convex lower bound. This means that when there are more degrees of freedom, the convex subset is no longer a good approximation of the entire KC C-space.

As a comparison over different aspect ratios, we fix the largest semi-axis of E_a as $a_1 = 4$, and the vary the other two semi-axis lengths by different aspect ratios, i.e. $a_2 = a_1/\alpha_1, a_3 = a_1/\alpha_2$, where $\alpha_1, \alpha_2 \in [1, 1.2]$. Figure 10 shows the comparison results. As the aspect ratios increase, which gives more constraints for E_a to move, the volumes

decreases, but the relative volumes are stable for both of the two lower bounds. Also, the geometric lower bound performs much better than the convex lower bound.
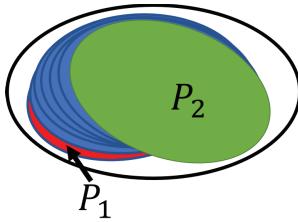
9 Applications

The kinematics of containment for ellipsoids has a wide range of real-life applications such as robot motion planning, parts-handling mechanisms, automated assembly, etc. For example, when planning a collision-free path for a mobile robot, the convex subspace of the allowable motions gives a solution for safe configuration connections; and when evaluating the robustness of a robot manipulator, the volume of the allowable motion space can be treated as a metric. Therefore, this section discusses the potential applications of the proposed theory, and provides some simple examples that might lead to the future work.
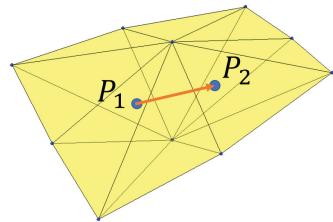
9.1 Safe Configuration Connections for Robot Motion Planning Problems

Generating a collision-free path is the essential goal and priority in robot motion planning problems, with PRM, RRT and their variants being efficient state-of-the-art planners. Generally speaking, those planners randomly generates vertices in the configuration space and checks for collisions in the Euclidean space. Once a collision-free configuration is found, it is stored in either a graph or tree data structure. Then, to connect those valid configurations into edges, interpolations between two configurations are often performed. Despite the fact of simplicity and effectiveness in practice, such edge connection strategies are discrete, which significantly depends on the resolution of interpolations. Therefore, it might not provide a safe guarantee for the edges, especially in the case of narrow passage. This is where the propose "Convex Lower Bound" of the KC C-space fits in.

Consider a 2D path planning problem for a holonomic elliptical robot, as illustrated in the introduction, and suppose the robot is enlarged by a small inflation. Then the actual robot can move slightly inside the larger ellipse, denoted here as a "guard". Once the vertex generations are performed with respect to the guard, all the allowable motions for the robot are guaranteed to be collision-free, and a KC C-space can be generated accordingly. Here, the "Con-

(a) The robot motions in the Euclidean space.

(b) Vertex connections in the configuration space.

Fig. 11: A demonstration of the configuration connection strategy. The robot is moving from P_1 to P_2 while staying fully contained in the larger ellipse (as shown in a). If the KC C-space is convex (as shown in b), then the path is guaranteed to be collision-free.

vex Lower Bound" plays a necessary role to connect adjacent configurations, since any path within the convex subspace is guaranteed to be safe. If the two adjacent configurations are both inside the convex lower bound, then connecting them remains simply to find a straight path between them. This provides a collision-free edge between the two configurations without interpolations and thus any collision checking calculation for the configurations between them. Figure 11 shows the idea of configuration connections within the convex lower bound of the KC C-space.

The KC theories and the vertex connection strategy described above have been applied and shown a success in 2D motion planning problems in [24], where the robot is encapsulated by an ellipse. As an extension of the motion planner, it is important to tackle the more difficult 3D problems with the similar ideas. Therefore this article deals with the general n-dimensional case (particularly verified when $n = 3$), and will provide a more useful tool for the motion planning algorithm in 3D.

9.2 Error Analysis for Robot Manipulators

The "pick-and-place" task is a famous problem for robot manipulators, where the accuracy of handling parts requires the control of errors from the joints. Because of the unavoidable errors propagated from the joints, the end effector of the manipulator always has uncertainties. Suppose that the object to be handled is enclosed by a 3D ellipsoid, with its center of mass being a reference point. Then a body-fixed reference frame can be attached to that point, which describes the configuration of the object, and all the possible configurations form a space of uncertain poses, denoted as "error space". In practice, the error space can be constructed numerically by encapsulating an ellipsoid to the object at some sample ending poses. The target placing location can be inscribed by another ellipsoid that is slightly larger than the object, in order to give some clearance to put the object.

Therefore, for such a "pick-and-place" task, it is always important to:
(I) determine whether the error space is fully contained in the target area; and

Table 2: Numerical settings of the error analysis for a pick-and-place task by KUKA LWR robot.

Description	Numerical Data
Ellipsoidal object	$\mathbf{a}_0 = [0.2, 0.15, 0.1]^\top$
Desired pose	$(R\vert\mathbf{t}) = \begin{pmatrix} 1 & 0 & 0 & 0.5 \\ 0 & -1 & 0 & 0 \\ 0 & 0 & -1 & 0.15 \end{pmatrix}$
Desired joint angles	$\mathbf{q} = [-0.7768, 0.1991, -0.1991,$ $1.6981, -1.6241, 1.9656, -0.9147]^\top$

(II) assess the robustness of the robot that can deal with error on its joints.

These two goals are closely related to the proposed theory, where the "Geometric Lower Bound" can be applied since it occupies larger volume in the C-space. The following example gives a numerical demonstration of how the two goals are addressed by using the theory of KC C-space, which is performed on a KUKA LWR robot shown in Fig. 1.

The simulation is performed by first setting a target pose, and solving for the corresponding configuration in the joint space [25]. The object is predefined with fixed semi-axes lengths, and the target area is slightly larger with a fixed inflation factor ε. To model the uncertainty, a zero mean Gaussian white noise is added to each joint angle. The simulation is repeated with different standard deviation of the noise, and at each trial, 100 random poses of the object are placed accordingly. Table 2 shows the numerical settings of this example.

Problem (I) can be addressed by directly querying whether the error space is inside the target area. The simulation results demonstrate the correspondence between the inflation factor and the uncertainty of each joint with different noise levels. The inflation factor for the target area is determined numerically as the minimum number that the object is placed safely inside the target at all the possible poses. This gives a guidance for the design of the control method to limit the error within an acceptable range.

To assess how much error the robot manipulator can deal with, as stated in problem (II), the concept of *parts entropy* [26] is used here as an evaluation metric. The parts entropy evolving in time t for one object is originally defined as

$$S_h(t) = -\int_G h(g;t) \log h(g;t) dg. \qquad (39)$$

For this application where the target is fixed and the object is moving, the distribution of the constrained motion of the object can be computed as $h(g) = 1/V$, where V is the volume of the allowable motion in PCG(3) [27]. The resulting parts entropy is therefore given by $S_h = \log V$. Since the volume is associated with the inflation factor, for each experimental trial, the parts entropy is computed. Figure 12 plots the relationships between the joint errors, inflation factors and the corresponding parts entropy.
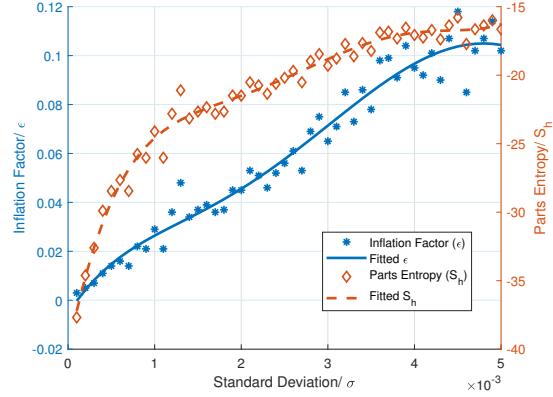
Fig. 12: Simulation result for the pick-and-place task.

The trend of the data points gives the relationships between the joint errors and robustness of the manipulator. As the error of each joint grows, the space to be placed needs to be larger to accommodate the noise, and so the parts entropy becomes larger also. In the real application, on one hand, once the control parameters of the manipulator are well-tuned, one can refer to this figure to determine how large the target area is; while on the other hand, if the target space is chosen in advance, one can also read from the figure and find the requirement for the errors of the joints, which guides the control strategy.

10 Conclusion

The fields of automated assembly and robot motion planning deal with many problems of determining whether one object is contained in another, and how much space the smaller object can move without any collision. This article applies the concept of the Kinematics of Containment and investigates a special case when the arena is slightly larger than the moving object, both of which are ellipsoids. The algebraic condition of containment is reviewed and the geometric condition of containment is then introduced. Based on these two conditions, two lower bounds for the allowable motion in the configuration space are proposed, denoted as *Convex Lower Bound* and *Geometric Lower Bound* respectively. Containment checking process for a specific configuration and volume of motions within the lower bounds are introduced. To verify the theory, implementations and volume comparisons in 2D ellipses and 3D ellipsoids cases are performed. The results show that the Geometric Lower Bound occupies larger volume in the C-space than the Convex Lower Bound when the smaller ellipsoid has more freedom to move, and its relative volume to the actual KC C-space performs more stable with the change of the ellipsoid shapes. Finally, applications on a configuration connection strategy for path planning problems and a pick-and-place task with uncertainties on the end effector of a manipulator are studied and numerically demonstrated.

Nomenclature

A The shape matrix for a general n-dimensional ellipsoid.

$C_{\mathbf{u}}(\cdot)$ A family of expressions for the approximation of the algebraic condition of containment, with $\mathbf{u}$ being the parameters.

$C_i(\cdot)$ i^{th} element in the family $C_{\mathbf{u}}(\cdot)$.

E_a The moving smaller ellipsoid A.

E_b The fixed larger ellipsoid B.

E_a' E_a after the shrinking transformation.

E_b' E_b after the shrinking transformation.

$\mathbb{I}$ Identity matrix.

K_a The moving smaller convex body.

K_b The fixed larger convex body.

P_i^s i^{th} vertex of a simplex in $\mathbb{R}^n$, where $i = 0, 1, ..., n$.

R A rotation matrix as an element in SO(n).

$S_h(t)$ Time-evolving parts entropy for probability $h(g;t)$.

T Transformation matrix for the shrinking operations.

V Volume of allowable motions.

$\mathbf{a}$ Semi-axis lengths of E_a, i.e. $\mathbf{a} = [a_1, a_2, ..., a_n]^\top$.

$\mathbf{b}$ Semi-axis lengths of E_b, i.e. $\mathbf{b} = [b_1, b_2, ..., b_n]^\top$.

d_i^* Extreme distance that a sphere can move along the ith semi-axis of an ellipsoid while remain fully contained.

$\mathbf{e}_i$ i^{th} basis element of a Cartesian coordinate system.

$f(\cdot)$ Any general function.

g A rigid-body motion, i.e. $g \in$ SE(n) $\doteq$ SO(n) $\ltimes \mathbb{R}^n$. Further, the group action can be denoted as $g \cdot K \doteq RK + \mathbf{t}$.

$h(g;t)$ Time-evolving probabilistic density function with respect to rigid-body motion.

m Number of finite sampling points in $\mathbb{R}^n$.

n Dimensions of the space.

$\mathbf{n}$ Unit normal vector of a surface.

$\mathbf{q}$ A vector of joint angles for a robot manipulator.

r Radius of E_a', which is shrunk into a sphere.

$\mathbf{t}$ Translation element in a rigid-body motion in $\mathbb{R}^n$.

$\mathbf{u}$ Explicit expression of an n-dimensional sphere with $\|\mathbf{u}\| = 1$.

$\mathbf{x}$ A general point in $\mathbb{R}^n$.

$\mathbf{x}_0$ A specific point for containment checking in $\mathbb{R}^n$.

$\mathbf{x}_{eb}$ A point on the Minkowksi difference boundary.

$\Lambda(\cdot)$ A diagonal matrix in $\mathbb{R}^{n \times n}$.

$\Phi(\cdot)$ Implicit expression of a surface in $\mathbb{R}^n$.

$\mathcal{A}(\cdot)$ Area of a planar body.

$\mathcal{P}(\cdot)$ Perimeter of a planar body.

$\mathcal{F}(\cdot)$ Surface area of bounding surface enclosing a spatial body.

$\mathcal{M}(\cdot)$ Integral of mean curvature of bounding surface enclosing a spatial body.

$\mathcal{V}(\cdot)$ Volume of a body in $\mathbb{R}^n$.

α The aspect ratio of an ellipsoid.

ε The positive inflation factor between two ellipsoids E_a and E_b, i.e. $\mathbf{b} = (1+\varepsilon)\mathbf{a}$.

ω An element in the Lie algebra $\mathfrak{so}(n)$, i.e. $\omega = \log^\vee(R) \in \mathbb{R}^{n(n-1)/2}$

ξ An element in the Lie algebra $\mathfrak{pcg}(n)$, i.e. $\xi = [\omega^\top, \mathbf{t}^\top]^\top \in \mathbb{R}^{n(n+1)/2}$.

θ_{exi} Extreme angle that an ellipsoid can rotate around i-th semi-axis of a larger ellipsoid without collisions.

$\iota(\cdot)$ An indicator function.

$\vee$ Vectorization operation for a skew-symmetric matrix.

$\widehat{\cdot}$ Hat operation that converts a vector into a skew-symmetric matrix.

$\|\cdot\|$ Euclidean norm of a vector.

$\top$ Transpose of a matrix or vector.

References

[1] Latombe, J.-C., 2012. *Robot motion planning*, Vol. 124. Springer Science & Business Media.

[2] Karnik, M., Gupta, S. K., and Magrab, E. B., 2005. "Geometric algorithms for containment analysis of rotational parts". *Computer-Aided Design,* **37**(2), pp. 213–230.

[3] Halperin, D., Latombe, J.-C., and Wilson, R. H., 2000. "A general framework for assembly planning: The motion space approach". *Algorithmica,* **26**(3-4), pp. 577–601.

[4] Pac, M. R., and Popa, D. O., 2013. "Interval analysis of kinematic errors in serial manipulators using product of exponentials formula". *IEEE Transactions on Automation Science and Engineering,* **10**(3), pp. 525–535.

[5] Kavraki, L. E., Svestka, P., Latombe, J.-C., and Overmars, M. H., 1996. "Probabilistic roadmaps for path planning in high-dimensional configuration spaces". *IEEE Transactions on Robotics and Automation,* **12**(4).

[6] LaValle, S. M., 1998. "Rapidly-exploring random trees: A new tool for path planning".

[7] Kuffner, J. J., and LaValle, S. M., 2000. "RRT-connect: An efficient approach to single-query path planning". In Robotics and Automation, 2000. Proceedings. ICRA'00. IEEE International Conference on, Vol. 2, IEEE, pp. 995–1001.

[8] Choi, Y.-K., Chang, J.-W., Wang, W., Kim, M.-S., and Elber, G., 2009. "Continuous collision detection for ellipsoids". *IEEE Transactions on visualization and Computer Graphics,* **15**(2), pp. 311–325.

[9] Jia, X., Choi, Y.-K., Mourrain, B., and Wang, W., 2011. "An algebraic approach to continuous collision detection for ellipsoids". *Computer Aided Geometric Design,* **28**(3), pp. 164–176.

[10] Iwata, S., Nakatsukasa, Y., and Takeda, A., 2015. "Computing the signed distance between overlapping ellipsoids". *SIAM Journal on Optimization,* **25**(4), pp. 2359–2384.

[11] Chirikjian, G. S., and Yan, Y., 2014. "The kinematics of containment". In *Advances in Robot Kinematics*. Springer, pp. 355–364.

[12] Ma, Q., and Chirikjian, G. S., 2015. "A closed-form lower bound on the allowable motion for an ellipsoidal body and environment". In IDETC/CIE, ASME, p. V05CT08A055.

[13] Blaschke, W., 1955. "Vorlesungen über integralgeometrie, deutsch". *Verlag Wiss., Berlin*.

[14] Sors, L. A. S., and Santaló, L. A., 2004. *Integral geometry and geometric probability*. Cambridge university press.

[15] Aubin, J.-P., and Frankowska, H., 2009. *Set-valued analysis*. Springer Science & Business Media.

[16] Chirikjian, G. S., Mahony, R., Ruan, S., and Trumpf, J., 2018. "Pose changes from a different point of view". *ASME. J. Mechanisms Robotics*.

[17] Lozano-Perez, T., 1983. "Spatial planning: A configuration space approach". *IEEE transactions on computers*(2), pp. 108–120.

[18] Yan, Y., and Chirikjian, G. S., 2015. "Closed-form characterization of the Minkowski sum and difference of two ellipsoids". *Geometriae Dedicata,* **177**(1), pp. 103–128.

[19] Kurzhanskiy, A. A., and Varaiya, P., 2006. "Ellipsoidal toolbox (ET)". In Decision and Control, 2006 45th IEEE Conference on, IEEE, pp. 1498–1503.

[20] Bertsekas, D. P., 2009. *Convex optimization theory*. Athena Scientific Belmont.

[21] De Berg, M., Van Kreveld, M., Overmars, M., and Schwarzkopf, O. C., 2000. "Computational geometry". In *Computational geometry*. Springer, pp. 1–17.

[22] Stein, P., 1966. "A note on the volume of a simplex". *The American Mathematical Monthly,* **73**(3), pp. 299–301.

[23] Chirikjian, G. S., 2011. *Stochastic Models, Information Theory, and Lie Groups, Volume 2: Analytic Methods and Modern Applications*, Vol. 2. Springer Science & Business Media.

[24] Ruan, S., Ma, Q., Poblete, K. L., Yan, Y., and Chirikjian, G. S., 2018. "Path planning for ellipsoidal robots and general obstacles via closed-form characterization of Minkowski operations". In WAFR: Proceedings of the Workshop on Algorithmic Foundations of Robotics.

[25] Corke, P., 2017. *Robotics, Vision and Control: Fundamental Algorithms In MATLAB® Second, Completely Revised*, Vol. 118. Springer.

[26] Sanderson, A., 1984. "Parts entropy methods for robotic assembly system design". In Robotics and automation. Proceedings. 1984 IEEE international conference on, Vol. 1, IEEE, pp. 600–608.

[27] Chirikjian, G. S., 2008. "Parts entropy and the principal kinematic formula". In CASE, IEEE, pp. 864–869.